

Large-Eddy Simulation of Flow Through a Low-Pressure Turbine Cascade

R. Mittal¹, S.Venkatasubramanian²

Department of Mechanical Engineering
University of Florida
Gainesville, Florida 32611

F.M. Najjar³

Center for Simulation of Advanced Rockets
University of Illinois at Urbana-Champaign
Urbana, Illinois 61801

ABSTRACT

The technique of large-eddy simulation (LES) has been used to simulate and analyze the flow through a low-pressure turbine (LPT) cascade. The objective of this study is to demonstrate the capability of LES to *predict* flow separation and the associated losses, and to analyze the spatio-temporal dynamics of the unsteady separation process. Simulations have been performed at Reynolds numbers (based on inlet velocity and axial chord) of 10000 and 25000. The focus of the current paper is to firstly describe the computational aspects of this study and secondly, to discuss the observed dynamics of the unsteady separation process at these relatively low Reynolds numbers.

1. INTRODUCTION

The current trend in the civil aviation industry is towards building increasingly compact and efficient engines. One component where increased blade loading and efficiency is being sought is the low-pressure turbine. The Reynolds numbers in the LPT at cruise can be lower by more than a factor of two at cruise as compared to takeoff. The lower Reynolds number makes the suction side boundary layer on the turbine blade more susceptible to separation and can lead to higher losses, lower stage efficiency and higher specific fuel consumption. In fact it has been found that efficiencies at cruise can be as much as two points lower than those at takeoff (Simon & Ashpis 1996). The separation process is highly unsteady and is significantly affected by factors such as Reynolds number, upstream rotor wakes and inlet turbulence (Qiu & Simon 1997, Schulte & Hodson 1998, Dorney & Ashpis 1999). Thus, the ability to accurately predict the separation induced losses and their dependence on these factors is of crucial importance in the design of an LPT blade. Investigation of this flow using ground test facilities is hampered to some extent by the inability to model cruise conditions. Thus, numerical modeling provides the

most promising and cost effective means of analyzing this flow configuration.

In the past, Reynolds-Averaged Navier-Stokes (RANS) modeling approaches have been used in order to analyze and predict the onset of separation in a LPT (Dorney et al. 1999, Chernobrovkin and Lakshminarayana 1999, Suzen et al. 2001). However, the boundary layer is transitional in nature and the transition location is not known a-priori. Furthermore, the separation process is highly unsteady with a wide variation in the separation location. Both these factors tend to limit the predictive capability of the RANS approach for this flow. Furthermore, conventional RANS simulations provide information only about the mean flow field and only limited insight regarding the dynamics of the unsteady separation process can be gained from these simulations.

In this context, the LES approach is better suited for this flow configuration. The LES methodology falls somewhere between the direct numerical simulation (DNS) and RANS (Moin 1991) approaches both in terms of the fidelity and computational expense. In LES, the large energy containing scales are resolved and only the effect of the small unresolved (subgrid) scales is modeled. Since these small motions are generally more homogeneous and universal, it is expected that a relatively simple SGS model will suffice. The Smagorinsky model (Smagorinsky 1963) is the simplest and most popular SGS model and has been used successfully in a variety of simple flows like isotropic turbulence, channel flows, etc. (Schumann 1975, Deardoff 1970). However, straightforward application of this model suffers from some of the deficiencies of the RANS approach namely, ad-hoc specification of model constants, need for a wall-model and inability to differentiate between laminar and turbulent regions of the flow. The development of the dynamic SGS model (Germano et al. 1991) has removed these constraints to a large extent. In this approach, a procedure for

¹Assistant Professor, member

²Graduate Student

³Research Scientist

dynamically calculating the model constant is added on to the SGS model (Germano et al. 1991, Moin 1991). As the calculation proceeds, the dynamic procedure utilizes information from the smallest resolved scales to predict the energy transfer to the subgrid scales. The model constant is then computed from the estimated rate of energy transfer. The dynamic model is ideally suited for complex flows since it automatically detects laminar subregions and turns itself off. Furthermore, it also provides the correct behavior near the wall thus obviating ad-hoc wall models (Moin et al. 1991). This modelling technique has been used successfully for simulating flows ranging from simple flows like flow in a channel to more complicated external and internal flows like bluff body wakes (Beaudan & Moin 1994, Mittal & Moin 1997) and flow in an asymmetric diffuser (Kaltenbach et al. 1999). Furthermore, this methodology has also been successfully used in predicting transition (Germano et al. 1991). More applications of this technique can be found in a recent review article by Piomelli (1999).

Thus, LES with the dynamic model has the potential of providing a robust predictive capability for the LPT flow. Furthermore, LES provides detailed time-dependent information about the important large scale features of the flow field without the immense cost of a DNS which would resolve all the scales down to the dissipation range. This is precisely the type of information that is required for understanding the detailed dynamics of the unsteady separating flow over a LPT blade. The objective of the current paper is to describe the application of an LES solver for this flow configuration at Reynolds numbers (based on the inlet velocity and axial chord) of upto 25000. The focus in the current paper is on describing the computational aspects of the simulations and the dynamics of the separation process at these relatively low Reynolds numbers.

2. NUMERICAL METHODOLOGY

Flow configuration. The flow configuration consists of a low-pressure turbine blade which has been the subject of a number of previous investigations (Murawski & Vafai 1999, Qiu & Simon 1999, Chernobrovkin & Lakshminarayana 1999). The interest here is in using LES to study the flow separation in the mid-span section of the blade where the flow is assumed to be homogeneous in the spanwise direction. Reynolds numbers (defined as $U_{in}C_a/\nu$ where U_{in} , C_a and ν are the inlet velocity, axial chord and kinematic viscosity respectively) of interest vary in the 10^4 – 10^5 range and inlet turbulence level ranges from about 0.3% to 10%. Furthermore, since it is also of interest to analyze the effect of upstream rotor wakes on the separation and transition process, these rotor wakes also have to be included in the numerical simulations. The current paper will however focus on describing the solver and results pertaining to cases with zero inlet turbulence level and no upstream rotor wakes. These simulations form the baseline for future simulations that would include these additional factors. Furthermore, inlet and exit Mach numbers in a typical LPT are limited to about 0.4 and 0.9 respectively. Thus, compressibility effects are present but it is expected that they do not have a significant effect on the separation process. The current simulations employ an

incompressible flow solver and therefore, compressibility effect are not included.

Governing Equation and SGS Model. In LES, the velocity and pressure fields are considered to be decomposed as $u_i = \bar{u}_i + u_i'$ and $p = \bar{p} + p'$ respectively, where the bar denotes large scales that can be resolved on a given mesh and the prime quantities are the subgrid scales, ie. scales that are smaller than the mesh size and therefore cannot be resolved. The above decomposition can be applied to the incompressible Navier-Stokes equations and the following “filtered” equations obtained for the resolved scales:

$$\frac{\partial \bar{u}_i}{\partial x_i} = 0 \quad (1)$$

$$\frac{\partial \bar{u}_i}{\partial t} + \frac{\partial \bar{u}_i \bar{u}_j}{\partial x_j} = - \frac{\partial \bar{p}}{\partial x_i} + \frac{1}{\text{Re}} \frac{\partial^2 \bar{u}_i}{\partial x_j \partial x_j} - \frac{\partial \tau_{ij}}{\partial x_j} \quad (2)$$

where τ_{ij} is the subgrid scale tensor given by $\tau_{ij} = \bar{u_i u_j} - \bar{u}_i \bar{u}_j$. The subgrid scale tensor cannot be calculated directly in a simulation since it requires knowledge of u_i and therefore of u_i' which is not known. Therefore, in order to close the above system of equations, a model needs to be used for the subgrid scale tensor. The most widely used subgrid scale stress model is an eddy-viscosity type model where $\tau_{ij} = (\delta_{ij}/3)\tau_{kk} = -2\nu_T \bar{S}_{ij}$. In this model, ν_T is the eddy-viscosity and \bar{S}_{ij} is the resolved strain-rate tensor. The Smagorinsky model (Smagorinsky 1963) is used to model the eddy viscosity where $\nu_T = (C_s \Delta)^2 |\bar{S}|$. In this model, C_s is the Smagorinsky constant which remains to be determined and Δ is a measure of the local grid spacing. The key to closing the above system of equations then is to obtain an appropriate value of the Smagorinsky constant C_s . Here we have used the spanwise averaged version of the dynamic model (Germano et al. 1991, Lilly 1992) for the parameterization of the subgrid scale stresses. In the dynamic model (Germano et al. 1991) a procedure is used which allows for the estimation of the Smagorinsky constant from the instantaneous resolved flow. Further details of this model are available in the references cited earlier. However, it is important to note that this model has a number of features that make it attractive for complex transitional and turbulent flow such as the one encountered in LPT. These include (a) no ad-hoc specification of model constants (b) no requirement for a wall model (c) automatic detection of laminar and turbulent regions and (d) capability to predict transition to turbulence. The last two are especially attractive for the flow in an LPT since the flow is transitional in nature with large variation in the transition location. Therefore, the ability to *predict* the onset of turbulence obviates the need for any ad-hoc assumptions regarding the transition process.

Spatial and Temporal Discretization. The 3-D governing equations (1) and (2) are cast in a generalized curvilinear coordinate system in the (x_1-x_2) plane whereas the x_3 direction is retained as a planar direction. A fully staggered arrangement of the primitive variables is used in the (x_1-x_2) plane and the equations are written in terms of the velocity fluxes on the cell faces. The spatial discretization scheme is a mixed finite-difference-spectral scheme where a second-order central

difference scheme is used in the (x_1-x_2) plane and a Fourier spectral method is used in the spanwise (x_3) direction. It is worth pointing out that the spatial discretization scheme used here is completely non-dissipative. Most Navier–Stokes codes employ some sort of numerical damping (by addition of explicit artificial viscosity or upwinding) in order to control aliasing errors and the associated non-linear instability. However, it has been shown (Mittal & Moin 1997) that numerical damping is highly undesirable in LES since this can overwhelm the contribution from the SGS eddy viscosity. Non-dissipative methods are therefore preferable for LES. However for non-dissipative schemes, aliasing error control has to be provided by means other than numerical damping. In the current spatial discretization the Fourier scheme is dealiased directly through a phase-shifting operation (Canuto et al. 1987). In the (x_1-x_2) plane, aliasing error is controlled by enforcing kinetic energy conservation (Kravchenko & Moin 1997). One disadvantage of using this scheme is the dominance of dispersive error which makes the simulation highly sensitive to aspects such as grid stretching and skewness. This issue will be discussed further in the following section.

A fractional-step scheme is used for advancing the solution in time. In this scheme the equations are advanced first to an intermediate step where only the convection and diffusion effects are taken into account. This is followed by the pressure correction step which requires the solution of the Poisson equation for pressure. Subsequently the pressure correction is added to the intermediate velocity field thereby resulting in a divergence free final velocity. A mixed implicit-explicit scheme is used for the advection-diffusion equation wherein a 3rd-order Runge-Kutta scheme is used for the non-linear convection and cross-terms and a Crank-Nicolson scheme is used for the diagonal viscous terms. This discretization scheme avoids the viscous stability constraints which can be quite restrictive for these types of computations. Further details regarding the numerical methodology can be found in Mittal & Moin (1997) and Kaltenbach et al (1999).

At the inlet, a uniform freestream velocity is prescribed at an angle of 55° from the vertical whereas a non-reflective boundary condition is used at the exit that allows vortex structures to convect out of the computational domain with minimal reflections. At the top and bottom boundaries a periodic boundary condition is imposed in order to model a blade cascade. The blade pitch is taken equal to $0.886C_a$.

3. COMPUTATIONAL ASPECTS

The $Re=10000$ simulation has been carried out on a $209 \times 191 \times 32$ ($x_1 \times x_2 \times x_3$) mesh which is shown in Figure 1. The spanwise domain size in this simulation is equal to $0.2C_a$. The mesh has been generated using the elliptic grid generator available in GRIDGENTM. It is desirable to choose the spanwise domain size as small as possible so as to reduce the cost of the simulation. At the same time, care should be taken to ensure that the domain size is large enough so as to not affect the results of the simulation. In order to demonstrate the adequacy of the chosen spanwise domain size, another simulation has been

performed at the same Reynolds numbers and mesh but with the spanwise domain size increased to $0.4C_a$. For the $Re=25000$ simulation two separate meshes with $257 \times 255 \times 48$ and $257 \times 287 \times 48$ points have been used. The spanwise domain size for these simulations is maintained at $0.2C_a$.

It is unlikely that the operating Reynolds number in a LPT would drop to the relatively low values chosen in the current study. However, these low Reynolds number simulations are invaluable in that they allow us to analyze the numerical issues encountered in the LES of this flow configuration on relatively coarse meshes. The knowledge gained from these simulations can then be used at higher Reynolds numbers which are of direct practical relevance. It should be pointed out that in a number of past investigations (Qiu and Simon 1997), the Reynolds number is defined based on the length of the suction surface and mean exit velocity. With such a non-dimensionalization, the Reynolds numbers of our simulations would correspond to roughly 24000 and 60000.

Figure 1 shows a 2-D view of the grid used for the $Re=10000$ simulation. This grid topology does not seem to be the most appropriate for this particular flow since the grid upstream and downstream of the blade is not aligned with the flow direction. This is particularly disadvantageous in the wake region since it is difficult to control the streamwise grid distribution. A better suited grid topology would be one in which the grid is aligned with the inlet and exit flow direction. However, use of such a grid with the current solver leads to some unexpected problems. The highly curved shape of the blade coupled with the need to have a periodic mesh in the crossflow direction, results in a mesh that is significantly skewed over the blade surface. In a mesh where the inlet and exit sections would be aligned with the nominal flow direction, the mesh skewness extends over the entire grid including the grid in the wake region. In contrast, for the type of mesh used in the current study the skewness is significant only over the blade surface and the upstream and downstream regions of the grid have relatively negligible skewness. It can be shown by analysis of the truncation error (as in Thompson et al. 1985) that for non-dissipative scheme such as the current second-order, central-difference scheme, a combination of grid skewness, streamwise grid stretching and large crossflow velocity component can lead to large dispersive errors and possibly even instability. For both types of grid, flow over the blade surface is not subject to large dispersive errors since despite significant grid skewness and stretching in the grid in this region, the crossflow velocity component is small due to the close proximity to the blade surface. However, for the grid which is aligned with the flow in the wake region, vortex structures convecting into this region produce a large crossflow velocity component. This leads to large dispersive errors which causes these vortex structures to distort and result in rapid growth in enstrophy. Thus, unless special techniques are devised to control this enstrophy growth, the grid topology used in the current study is most appropriate for LES of highly curved blades with non-dissipative schemes.

The solver has been ported to the Origin-2000 platform and parallelized using OpenMP. Figure 2 shows the scaleup achieved

on a $256 \times 256 \times 64$ grid on upto 16 processors. Final simulations have been carried out on 8 processors where a scaleup factor of roughly 6.9 is achieved. For a short time-interval at the beginning of each simulation, a small spanwise perturbation is provided at the inlet to initiate the growth of spanwise instabilities in the boundary layer. The flow is then allowed to develop naturally with no external perturbations. Eventually the flow reaches a stationary state and the simulation is continued further beyond this stage for at least $5C_a/U_{in}$ time units and statistics compiled over this time interval. One complete simulation for the $Re=25000$ case requires over 8000 (1-node) CPU hours.

4. DISCUSSION OF RESULTS

In Figure 3 are plotted mean velocity profiles on the suction surface at various chordwise locations for the two $Re=10000$ simulations that have been carried out. The plot indicates that the domain size has a limited effect on the flow near the trailing edge. It is expected that this effect will become more pronounced further downstream in the wake region with the growth in the size of the vortex structures. However, since the interest in the current study is on the analyzing the flow over the turbine blade, a spanwise domain size of $0.2C_a$ is sufficient. Furthermore, since at higher Reynolds numbers, the separation bubble is expected to reduce in size, a spanwise domain size of $0.2C_a$ will be more than sufficient.

In Figure 4, a sequence of spanwise averaged, spanwise vorticity plots and corresponding streamline plots pertaining to the $Re=10000$ simulations (with spanwise domain size of $0.2C_a$) are shown. The plots span a time-interval of about one time unit. The plots clearly show that the laminar boundary layer on the suction surface separates and rolls up into large, clockwise rotating vortices which subsequently convect down the blade surface and interact with the shear layer from the lower surface. The boundary layer separating from the pressure side at the trailing edge also rolls up into compact counter-clockwise rotating vortices and the flow downstream of the trailing edge shows some of the features of a classic Karman vortex street. Figure 5 shows contours of $\langle u_3^2 \rangle$ which is the spanwise normal fluctuating stress. This quantity marks regions where there is significant three-dimensionality. Since the spanwise normal stress is significant only beyond $x/C_a \approx 0.9$, this implies that the vortices on the suction side are almost perfectly two-dimensional when they are formed and develop three-dimensional variations only as they approach the trailing edge. This development of three-dimensionality is the first stage in the transition process which will eventually lead to the formation of a turbulent wake.

Figure 6 shows the temporal variation of u_1 along various location on the suction surface as well as in the very near wake, and 7 shows the corresponding frequency spectra. Based on the spectra of the first three probes which are located on the suction surface, we find that the non-dimensional frequency of vortex formation ($\Omega = fC_a/U_{in}$ where f is the frequency) is in the range from 1.0 to 1.17. However the last probe which is located in the very near wake, shows a dominant peak in the spectra at $\Omega = 2.14$ which is roughly twice the frequency observed on the

suction surface. Based on our simulations, we hypothesize that this doubling of frequency is due to the shedding of vortices from the pressure side which also form at the same frequency as the suction side vortices but are 180 degrees out of phase in the shedding cycle. This is precisely the scenario observed in the case of Karman vortex shedding from a bluff body. Finally, it is also worth noting that none of the spectra show any indications of an inertial-subrange thereby confirming that at this low Reynolds number, the flow over the suction surface as well as that in the near wake is not turbulent.

Figure 8 shows a comparison of the mean velocity profiles on the suction surface for the $Re=10000$ and 25000 simulations. Due to the presence of thin boundary and shear layers, it is critical to provide adequate grid resolution in the direction normal to the wall. In order to investigate the grid dependency of the computed results for the higher Reynolds number simulation, we have therefore carried out another simulation where the grid resolution in the wall normal direction is improved by adding 33 more points. The grid distribution in the other directions is kept the same. The fine mesh simulation however, is not fully converged yet and therefore, only limited conclusions can be drawn regarding the grid dependence.

A comparison of the mean velocity profiles for the two $Re=25000$ simulations indicates that the wall normal grid resolution does have a noticeable effect on the size and extent of the separation bubble. In particular, increase in resolution seems to reduce both the vertical and streamwise extent of the bubble. In general however, comparison with the $Re=10000$ profiles clearly indicates that as expected, the separation bubble is much smaller at the higher Reynolds number. In the rest of the paper, the results presented for the $Re=25000$ case correspond to the fully converged simulation on the $257 \times 255 \times 48$ mesh.

Figure 9 shows streamlines corresponding to the time and span averaged flow for $Re=10000$ and 25000 cases and this allows us to directly compare the size and structure of the mean recirculation bubble on the suction surface. For $Re=10000$, the recirculation zone extends from about $x/C_a = 0.69$ to the trailing edge whereas for $Re=25000$, the separation bubble extends from about $x/C_a = 0.71$ to the trailing edge. The more significant difference is in the wall-normal extent of the separation bubble. At the location where the separation bubbles have the largest wall-normal extent, the bubble extends about $0.08C_a$ from the blade surface for the $Re=10000$ case where as for the $Re=25000$ case, it extends to only about $0.03C_a$.

The total width of the wake (\mathcal{W}) for the $Re=10000$ simulation can be estimated as the maximum wall-normal extent of the separation bubble plus the blade thickness at this location and this is roughly about $0.11C_a$. If the dominant frequency in the wake is nondimensionalized as $f\mathcal{W}/U_{in}$, this gives a wake Strouhal number of roughly 0.23 which is clearly in line with the vortex shedding Strouhal numbers observed in the wake of bluff bodies (Roshko 1955). This provides further evidence that at least at these low Reynolds numbers, the dynamics of the separation phenomenon on the suction surface is governed by the Karman vortex shedding type behavior in the wake. Since this vortex shedding cannot occur without the vortices that are shed

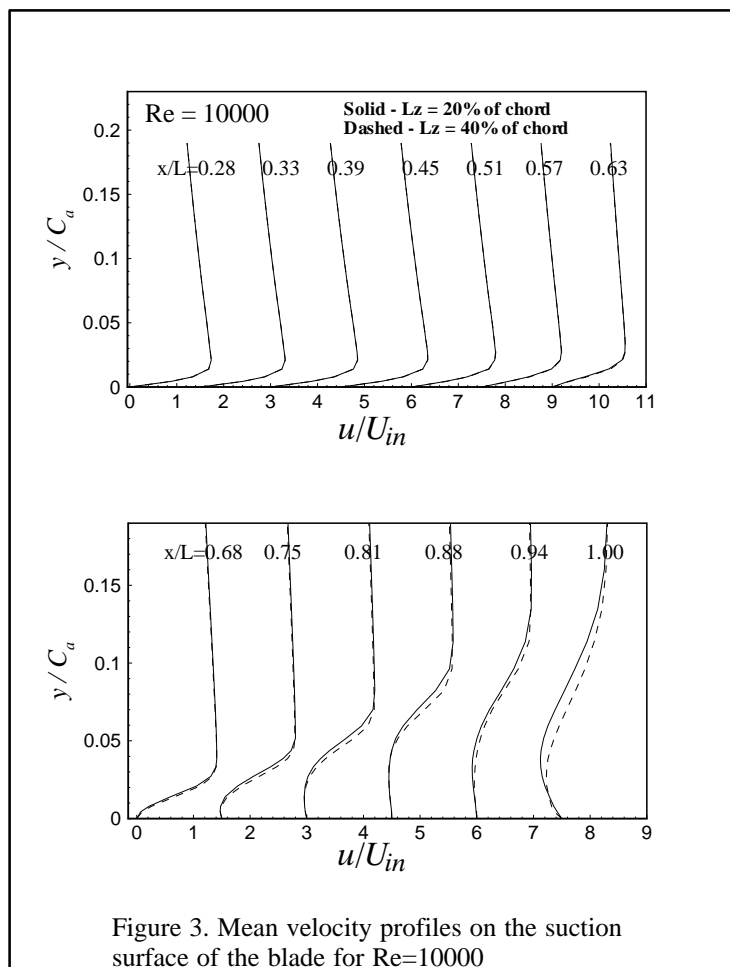
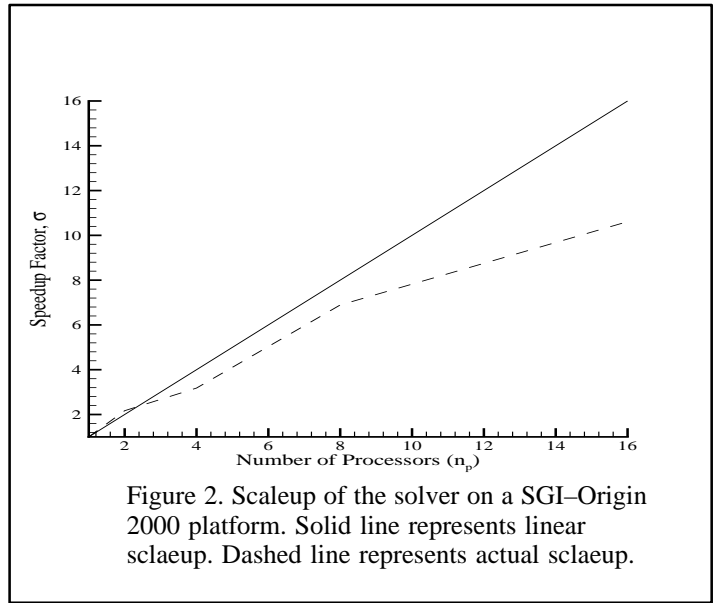
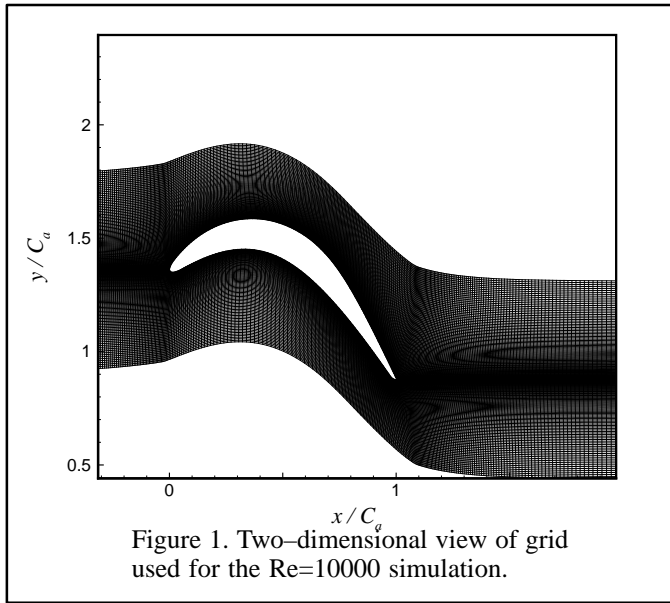
from the pressure side, accurate representation of the pressure side boundary layer is required in order to capture the dynamics of the separation on the suction side. Thus, “modeled” or “simulated” LPT configurations employed in some experiments (Qui & Simon 1997, Sohn et al. 1998), which do not include the pressure side of the blade, might not be able to capture this feature of the flow. However, it is likely that as the Reynolds number increases, the separating shear layer on the suction surface comes to be governed more by a Kelvin-Helmholtz type shear layer instability which is not strongly influenced by the vortex structures formed from the pressure side boundary layer. This hypothesis is being explored for the $Re=25000$ simulation and these results will be presented elsewhere.

ACKNOWLEDGEMENTS

This work was supported by Pratt & Whitney, East-Hartford, CT. Initial development of the LES solver was also supported by ONR Grant N00014-99-1-0389-P00002. Computer time for parallelizing the solver was provided by a supercomputing grant from NCSA at The University of Illinois at Urbana-Champaign.

REFERENCES

1. Beaudan, P. and Moin, P. (1994) Numerical Experiments on the Flow Past a Circular Cylinder at Sub-Critical Reynolds. Report. No, TF-62, Department of Mechanical Engineering, Stanford University.
2. Canuto C, Hussaini, MY, Quarteroni, A. and Zang, TA (1987) *Spectral Methods in Fluid Dynamics*. Springer-Verlag.
3. Chernobrovkin, A. & Laxminarayana, B. (1999) Turbulence Modeling and Computation of Viscous Transitional Flows for Low Pressure Turbines. *J. Fluids Engr.* Vol 121, P. 824.
4. Deardorff, JW (1970) A Numerical Study of Three-Dimensional Turbulent Channel Flow at Large Reynolds Numbers, *J. Fluid Mech.*, Vol. 41, Part 1, pp. 81-139.
5. Dorney, DJ, Ashpis, DE, Halstead and Wisler, DC (1999) Study of Boundary Layer Development in a Two-Stage Low-Pressure Turbine, *NASA/TM-1999-208913*.
6. Dorney, DJ and Ashpis, DE (1999) Study Of Low Reynolds Number Effects On The Losses In Low-Pressure Turbine Blade Rows, *J. Propulsion*, Vol. 16, No. 1 : Technical Notes.
7. Germano, M., Piomelli, U., Moin, P. and Cabot, W. (1991) A Dynamic Subgrid-Scale Eddy-Viscosity Model. *Physics of Fluids*, A 3 , pp. 1760-1765.
8. Kaltenbach, H-J, Fatica, M., Mittal, R., Lund, T.S. and Moin, P. (1999) Study of Flow in an Asymmetric Planar Diffuser using Large-Eddy Simulation, to appear in *J. of Fluid Mech.* 390, 151-186.
9. Kravchenko, AG, Moin, P. (1997) On the effect of Numerical errors in large-eddy simulations of turbulent flows. *J. Comp. Phys.* 131 (2) 310-322.
10. Lilly, D. K. (1992) “A Proposed Modification of the Germano Subgrid-Scale Closure Method,” *Physics of Fluids*, A4, pp. 633-635.
11. Mittal, R. and Moin, P. (1997) Suitability of Upwind-Biased Schemes for Large-Eddy Simulation of Turbulent Flows, *AIAA Journal*, Vol. 36, No. 8, pp 1415-1417.
12. Moin, P (1991) Towards Large Eddy and Direct Simulation of Complex Turbulent Flows, *Comput. Meth. Appl. Mech. Eng.* 87 (2-3): 329-334.
13. Murawski, CG & Vafai, K (1999) Effect of Variable Axial Chord on a Low-Pressure Turbine Blade, *J. Propul. Pow.* Vol. 15, No. 5, pp. 667-674.
14. Piomelli, U. (1999) Large-eddy simulation: achievements and challenges. *Prog. Aerosp. Sci.* 35 (4): 335-362.
15. Qiu, S. & Simon, TW (1997) An Experimental Investigation of Transition as Applied to Low Pressure Turbine Suction Surface Flows. *ASME 97-GT-455*.
16. Rogallo, RS and Moin P. (1984) Numerical Simulation of Turbulent Flows, *Annu. Rev. Fluid Mech.* 16, pp. 99-137.
17. Roshko, A. (1955) On the drag and shedding frequency of bluff-bodies, *J. Aero. Sci.* 22, 124-130.
18. Schumann (1975) Subgrid Scale Model for Finite Difference Simulations of Turbulent Flows in Plane Channels and Annuli, *J. Comp. Phys.* 18, pp. 376-404.
19. Schulte, V and Hodson, HP (1998) Unsteady Wake-Induced Boundary Layer Transition in High Lift LP Turbines, *Journal of Turbomachinery* Vol.120, pp. 28-35.
20. Simon, FF & Ashpis, DE (1996) Progress in Modeling of Laminar to Turbulent Transition on Turbine Vanes and Blades. *NASA TM 107180*.
21. Smagorinsky, J. “General Circulation Experiments with the Primitive Equations. I The Basic Experiment,” *Monthly Weather Review*, 91, 1963, 99-164.
22. Sohn, K-H , Shyne, RJ and DeWitt, KJ (1998) Experimental Investigation of Boundary Layer Behavior in a Simulated Low Pressure Turbine, *NASA/TM-1998-207921*.
23. Suzen, Y. B., Huang, P. G., Hultgren, L. S. and Ashpis, D. E. (2001) Predictions of Separated and Transitional Boundary Layers Under Low-Pressure Turbine Airfoil Conditions Using an Intermittency Transport Equation, *AIAA Journal* 2001-0446.
24. Thompson, JF, Warsi, ZUA, Mastin, CW (1985) *Numerical Grid Generation Foundation and Applications*. North-Holland.



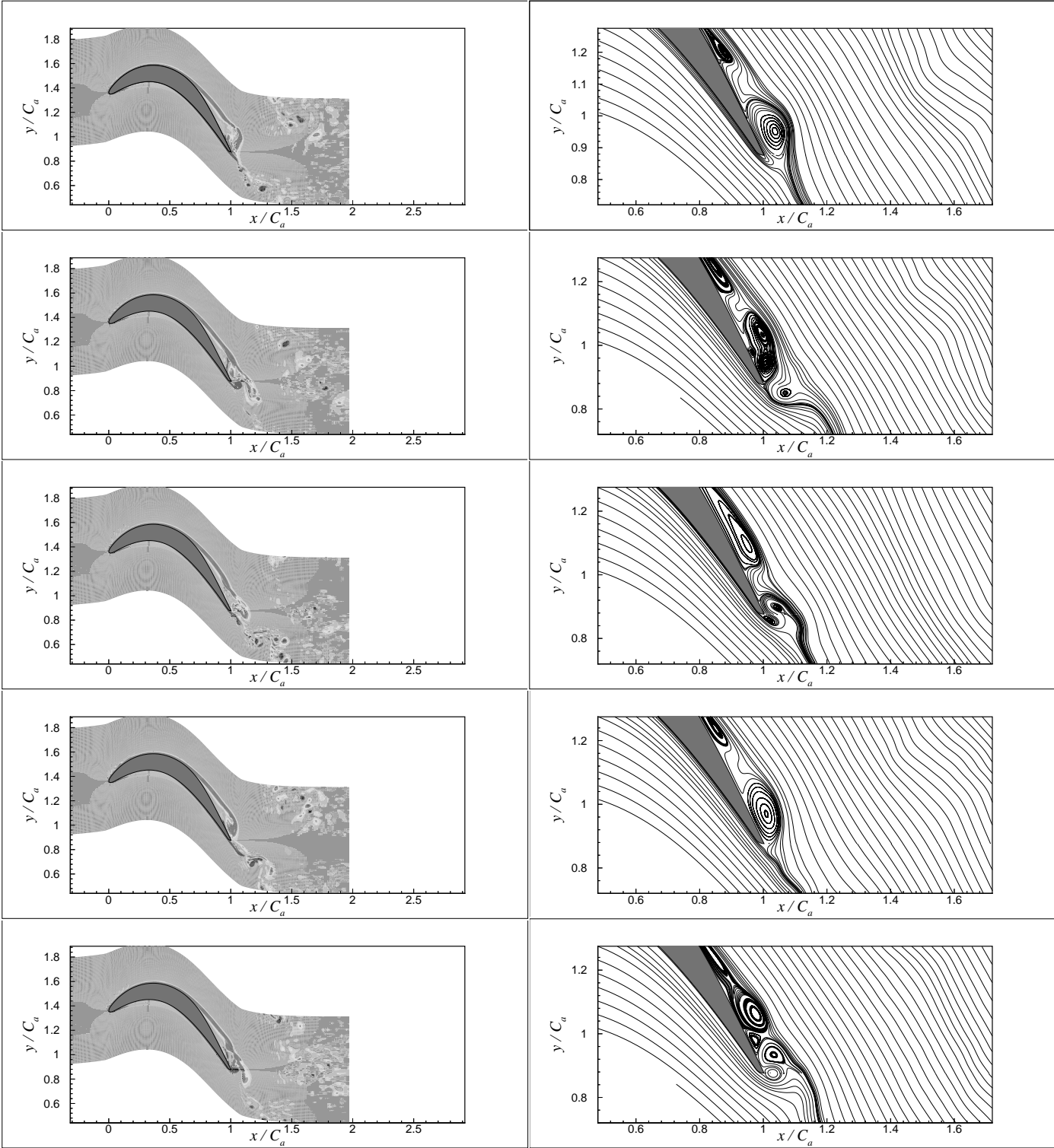


Figure 4. Sequence of vorticity and streamline plots over one flow cycle for Re=10000 simulation. (a) $t/T = 21.14$ (b) $t/T = 21.30$ (c) $t/T = 21.63$ (d) $t/T = 21.90$ (e) $t/T = 22.15$

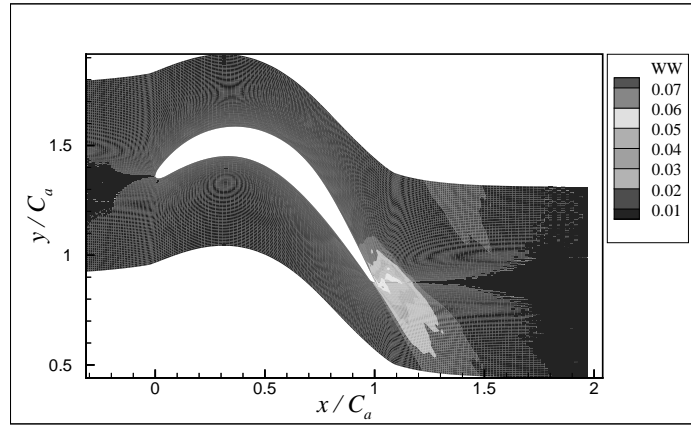


Figure 5. Countour plot of the spanwise normal fluctuation stress for the Re = 10000 simulation.

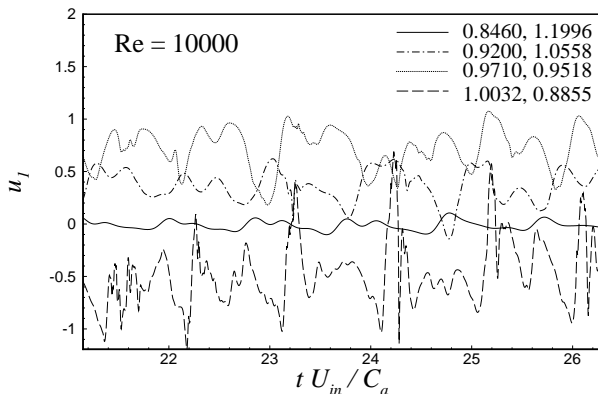


Figure 6. Temporal variation of streamwise velocity. The plots have been offset in the vertical direction. (a) $x/L=0.81$; offset=+0 (b) $x/L=0.93$; offset=+0.35 (c) $x/L=1.02$; offset=+0.85 (d) $x/L=1.08$; offset=-0.45

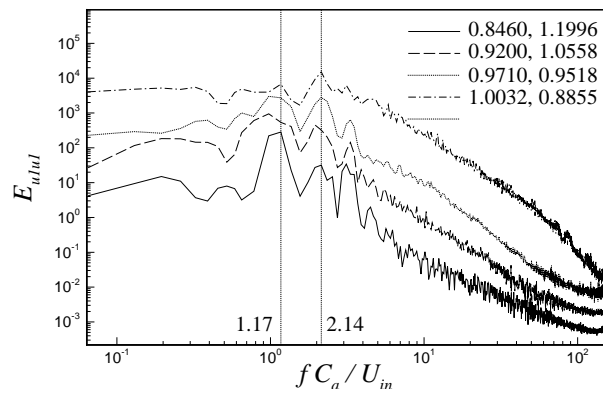


Figure 7. Frequency spectra corresponding to the velocity variations in Figure 4. The spectra have been offset in the vertical direction. (a) $x/L=0.81$; offset=x1 (b) $x/L=0.93$; offset=x6 (c) $x/L=1.02$; offset=x25 (d) $x/L=1.08$; offset=x155

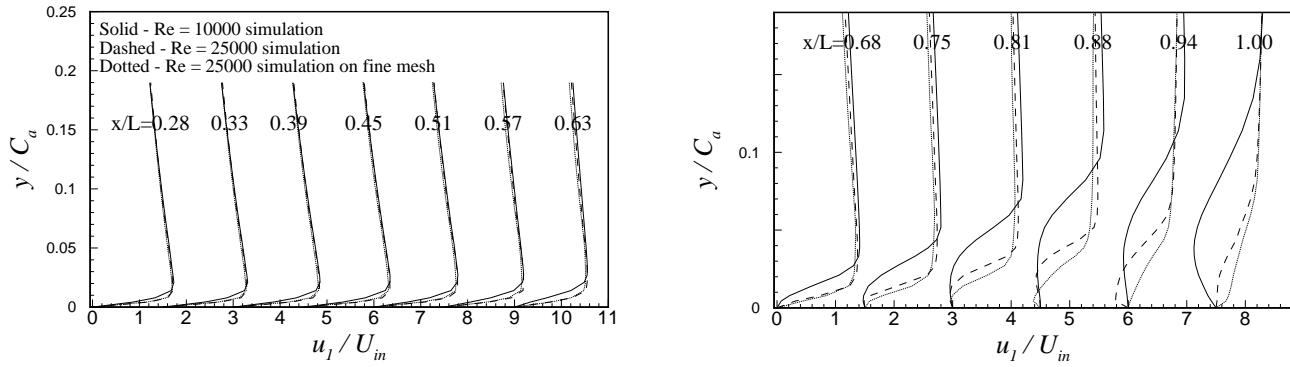


Figure 8. Streamwise velocity profiles for the Re = 10000 and the Re = 25000 simulations on the suction surface. The profiles have each been offset in the horizontal direction by 1.5.

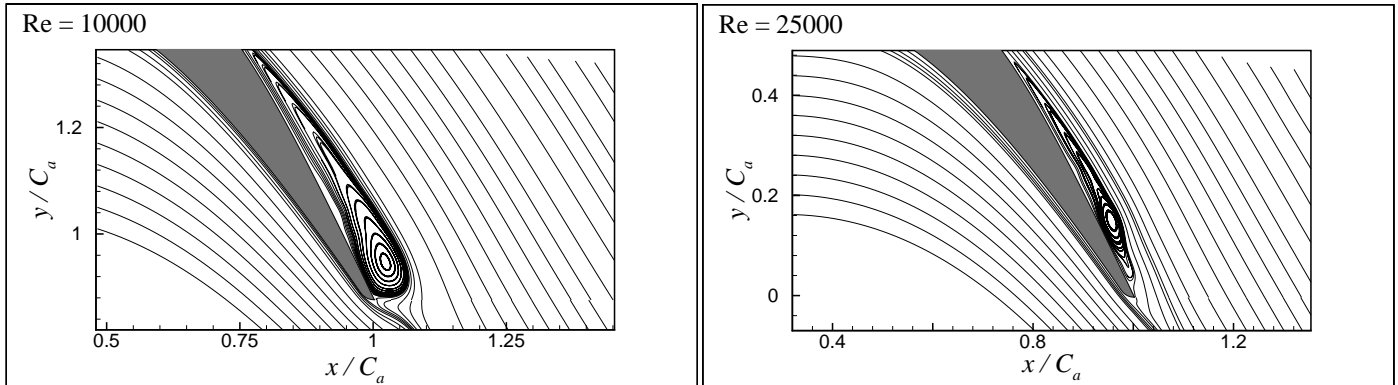


Figure 9. Mean streamline plots showing the separation bubble (a) Re = 10000 simulation (b) Re = 25000 simulation.